# Image-Based Control of Two Mobile Robots for Object Pushing

Gonzalo López-Nicolás, Erol Özgür and Youcef Mezouar

*Abstract*— **This paper shows how to push an unknown object in the plane from an initial pose to a target pose with two co-operating mobile robots. On the object motion, we deliberately impose non-holonomic velocity constraint with pushing mobile robots. This yields smooth and efficient trajectories. Pushing manipulation is performed, for the first time, with a new uncalibrated image-based control scheme. This is achieved by transforming the image information to a scaled Euclidean space without using any metric information or calibration. Stability of the control law is also demonstrated.**

## I. INTRODUCTION

The task of moving an object in robotics is usually performed by grasping. However, sometimes the robot lacks the size to grasp or the strength to lift the object. This problem can be overcome by moving the object by pushing. Moreover, since one robot may have not enough power to push the object, a multi-robot approach has been considered. Here, we propose a new visual servoing control law for pushing an object in a multi-robot framework.

In the literature, there have been exhaustive studies on moving objects by pushing: Mason was the first to study the mechanics of pushing [1]. Pushing is mainly served in two ways: (i) to remove uncertainty in the pose of an object before grasping it [1], [2], [3] or (ii) to move an object from one pose to another [4], [5]. Related works can be grouped into open-loop [6], [7] or closed-loop [8], [9], [10], [11] approaches with single point contact push [10], two point contacts push [11], line contact push [12] or multiple contacts push [13], [14], [15].

This paper proposes a new solution to the problem of pushing an object in the plane to a desired pose. We push the object with two mobile robots. Robots and the object interact with each other through frictional point contacts. We constrain the object with these frictional point contacts to move like a non-holonomic vehicle actuated only for forward motion. By doing so, we can exploit the well-studied contact physics and the non-holonomic vehicle kinematics theories to model and control the pushing. Afterwards, we perform the pushing by using only the image information obtained from an uncalibrated camera looking to the workspace. The

G. López-Nicolás is with Instituto de Investigación en Ingeniería de Aragón. Universidad de Zaragoza, Spain. `gonlopez@unizar.es`

E. Özgür is with Universite d'Auvergne (ISIT - ALCoV), Clermont-Ferrand, France. `erol.ozgur@udamail.fr`

Y. Mezouar is with Institut Pascal, UBP/IFMA/CNRS, Clermont-Ferrand, France. `Youcef.Mezouar@ifma.fr`

advantage of uncalibrated approaches is that their results do not depend on the quality of the system calibration and are more robust to system degradation. Therefore, we avoid using the camera calibration or additional information, such as the size of the object or its 3D model.

Similar to [7], we consider the following assumptions for the pushing task definition: (i) All motions and forces are in an obstacle-free plane which is normal to the gravity vector. (ii) Frictional forces conform to Coulomb's Law. (iii) The friction is uniform between the object and the support plane. This means that the center of friction of the pushed object is the point in the support plane beneath the center of mass of the pushed object. (iv) Motions are slow enough that inertial forces are negligible, i.e., quasi-static motion assumption.

The contribution of this paper is an uncalibrated image-based control scheme to manipulate objects by pushing under non-holonomic velocity constraint. First, we define a new procedure to transform the image information to a scaled Euclidean space with the novelty that we do not need to use any metric information, calibration, or 3D model of the object. Secondly, we propose a new control scheme for pushing with two mobile robots which yields smooth and efficient trajectories. The proposed control strategy is inspired from [16]. In particular, the control law in [16] was defined for a single mobile robot equipped with a calibrated camera on board, whereas here we use uncalibrated image information from an external camera looking to the scene, and then apply it to a system composed by two mobile robots and the object to be pushed. Finally, constraints on the system are studied and stability of the control law is proven. Simulations show the validity of the approach.

## II. FROM PROJECTIVE TO SIMILARITY SPACE

Since we propose an uncalibrated approach to manipulate an unknown object, we cannot recover the metric values of the object state as in [17]. However, we can still correct the distorted angles and recover the distances up to a scale by transforming the image points from projective space to a similarity space, i.e., scaled Euclidean space. This will be enough to fulfill our task.

The control task requires a target image with the object in the desired pose and the image of the object in the current position. Given enough correspondences between the target and current object features (e.g., points), we know how to compute a homography matrix $\mathbf{H}$ which maps the target object points $\mathbf{p}_T$ to the corresponding current object points $\mathbf{p}_C$ up to a scale in the measurable image plane $\pi_I$:

$$\mathbf{p}_C = \mathbf{H}\,\mathbf{p}_T, \qquad \{\mathbf{p}_C, \mathbf{p}_T\} \in \pi_I \qquad (1)$$

where $\mathbf{H}$ is as follows:

$$\mathbf{H} = \begin{bmatrix} h_{11} & h_{12} & h_{13} \\ h_{21} & h_{22} & h_{23} \\ h_{31} & h_{32} & h_{33} \end{bmatrix} \quad (2)$$

After this step, to recover back the undistorted angles, we do an affine rectification. That is to say, we relate the target object to the current object by an affine transformation $\mathbf{A}$ in an affine plane $\pi_A$. This can be done by a computable matrix $\mathbf{H}_A$ which maps the features from the measurable image plane $\pi_I$ to the affine plane $\pi_A$. In order to compute $\mathbf{H}_A$, we exploit the following expression:

$$\mathbf{A} = \mathbf{H}_A \, \mathbf{H} \, \mathbf{H}_A^{-1} \quad (3)$$

where the structure of $\mathbf{A}$ and $\mathbf{H}_A$ are given as below:

$$\mathbf{A} = \begin{bmatrix} a_{11} & a_{12} & b_1 \\ a_{21} & a_{22} & b_2 \\ 0 & 0 & 1 \end{bmatrix}, \quad \mathbf{H}_A = \begin{bmatrix} 1 & 0 & 0 \\ 0 & 1 & 0 \\ \ell_1 & \ell_2 & 1 \end{bmatrix} \quad (4)$$

The unknown variables $\ell_1$ and $\ell_2$ of $\mathbf{H}_A$ are computable from the two constraints ($a_{31} = 0$ and $a_{32} = 0$) of (3) which are written explicitly as follows:

$$h_{31} - \ell_1 \, (h_{33} + h_{13} \, \ell_1 + h_{23} \, \ell_2) + h_{11} \, \ell_1 + h_{21} \, \ell_2 = 0$$
$$h_{32} - \ell_2 \, (h_{33} + h_{13} \, \ell_1 + h_{23} \, \ell_2) + h_{12} \, \ell_1 + h_{22} \, \ell_2 = 0 \quad (5)$$

Then, we do Euclidean rectification. That is to say, we relate the target object to the current object by an Euclidean transformation $\mathbf{E}$ in a similarity plane $\pi_S$ (i.e., scaled Euclidean plane). This can be done by a computable matrix $\mathbf{H}_S$ which maps the features from the affine plane $\pi_A$ to the similarity plane $\pi_S$. In order to compute $\mathbf{H}_S$, again similar to previous step, we exploit the following expression:

$$\mathbf{E} = \mathbf{H}_S \, \mathbf{A} \, \mathbf{H}_S^{-1} \quad (6)$$

where the structure of $\mathbf{E}$ and $\mathbf{H}_S$ are given as below:

$$\mathbf{E} = \begin{bmatrix} r_{11} & r_{12} & t_1 \\ r_{21} & r_{22} & t_2 \\ 0 & 0 & 1 \end{bmatrix}, \quad \mathbf{H}_S = \begin{bmatrix} m_1 & 0 & 0 \\ m_2 & m_3 & 0 \\ 0 & 0 & 1 \end{bmatrix} \quad (7)$$

The unknown variables $m_1$, $m_2$ and $m_3$ of $\mathbf{H}_S$ are computable from the constraints of (6) which are shown implicitly using the components of the rotational matrix part of $\mathbf{E}$ as follows:

$$\begin{aligned} r_{11} - r_{22} &= 0 \\ r_{12} + r_{21} &= 0 \\ r_{11} \, r_{22} - r_{12} \, r_{21} &= 1 \end{aligned} \quad (8)$$

Now, we can bring the measured image points from an image plane to a scaled Euclidean plane as below:

$$\bar{\mathbf{p}} = \mathbf{H}_S \, \mathbf{H}_A \, \mathbf{p}, \qquad \bar{\mathbf{p}} \in \pi_S, \ \mathbf{p} \in \pi_I \quad (9)$$

We again note that a similarity plane $\pi_S$ preserves the angles, but the distances are up to an unknown scale. This unknown scale also changes with respect to current object pose. We need to fix this scale to a constant value so that stability of the control law defined in the following sections is guaranteed. In order to keep the unknown scale constant,
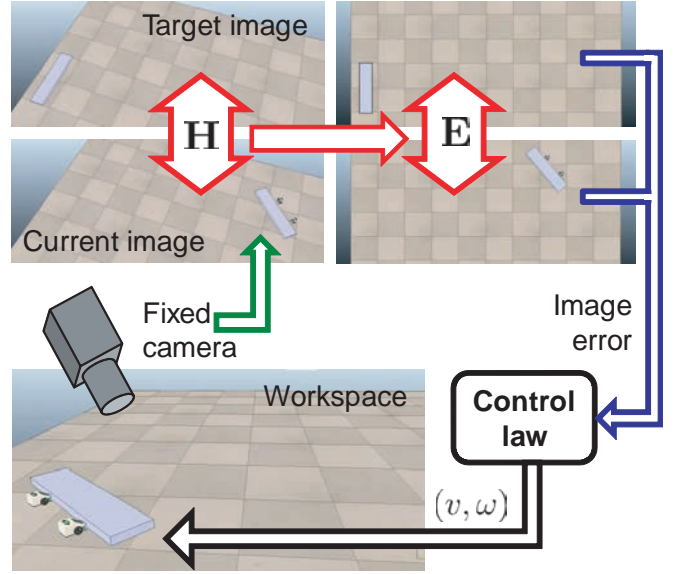


Fig. 1. Overview of the framework for visual servoing by pushing. A fixed camera observes the workspace, where two robots will push an object, and provides the current image to the visual loop. A homography $\mathbf{H}$ is computed from point matches on the object in the current and target views. Image points are then transformed so as to be related by $\mathbf{E}_S$. State of the object in these transformed images gives the image error to be corrected by the control law. Control law computes and sends to robots their velocities so that they push the object to the target location.

we transform the similarity plane $\pi_{S(t)}$ at time $t$ back to the first similarity plane $\pi_{S(t_0)}$ at time $t_0$ by a computable matrix $\mathbf{E}_S$. Given the corresponding points of the target object in two similarity planes $\pi_{S(t)}$ and $\pi_{S(t_0)}$, we can compute this scaled Euclidean transformation $\mathbf{E}_S$ which maps the target object from $\pi_{S(t)}$ to $\pi_{S(t_0)}$. The computed $\mathbf{E}_S$ has the following form:

$$\mathbf{E}_S = \begin{bmatrix} \mathbf{R}_S & \mathbf{t}_S \\ 0 & 1 \end{bmatrix} \quad (10)$$

where $\mathbf{R}_S$ is a rotation plus scale matrix. The final step is then to transform the features from $\pi_{S(t)}$ back to the $\pi_{S(t_0)}$:

$$\bar{\mathbf{p}}_{t_0} = \mathbf{E}_S \, \bar{\mathbf{p}}_t \quad (11)$$

A summary of the framework for visual servoing by pushing is shown in Fig. 1. This includes the proposed method for projective to similarity space transformation and the control scheme presented in the remainder of the paper.

## III. ACTUATION BY PUSHING WITH TWO FRICTIONAL POINT CONTACTS

Next, we propose a new control scheme for pushing with two mobile robots which yields smooth and efficient trajectories. We first address the model of the system in this section and the control design in the following.

The dynamics of multi-agent system manipulation has been investigated in [18]. In particular, they model the dynamics of pushing system under two agents. They also consider the case when both agents push in parallel so the reaction forces are always on the same direction. Here, we propose to model this particular system with the kinematics
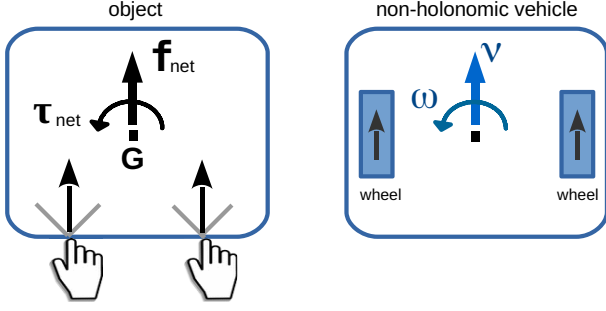
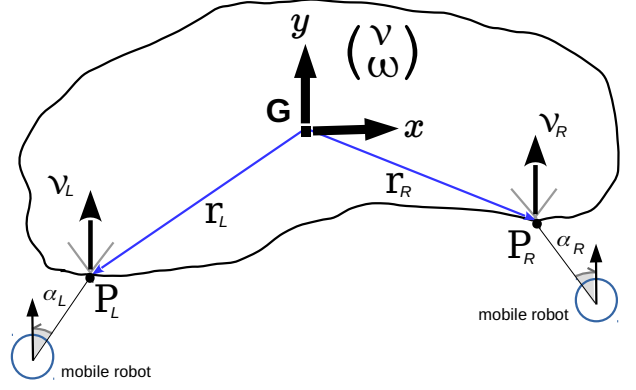Fig. 2. Moving an object like a non-holonomic vehicle by pushing.



Fig. 3. Geometry of the object with two pushing points. This can be considered as a pseudo non-holonomic vehicle with only forward motion.

of a nonholonomic vehicle. Note that without appropriate motion strategy, the object can actually translate in any direction. Then, in order to guarantee the validity of this model, an adequate control law should be designed to enforce the system to behave like a driftless nonholonomic system.

Since the object will be controlled by pushing, we first explain the physics of a frictional point contact, and then show how to actuate the object by pushing with two frictional point contacts like a non-holonomic vehicle. In a point contact with Coulomb friction model, the pusher can apply a force $\mathbf{f}$ to an object in any direction as long as it is oriented within the friction-cone. The apex of the friction-cone coincides with the contact point, and the cone axis is aligned with the inward object boundary normal. The cone aperture is defined by the static friction coefficient $\mu > 0$, see Fig. 2.

Exploiting the above frictional point contact physics, we now would like to move an object like a non-holonomic vehicle by pushing as it is illustrated in Fig. 2. In order to do so, we should push the object from points located on the left and right sides of its mass center $\mathbf{G}$, and each contact friction cone should allow to generate a force oriented towards the desired motion direction of the object. Afterwards, we know that from Newton's second law, if the mass of the object is constant, then the acceleration of the object is directly proportional to the net force and torque acting on the object and it is in the direction of the net force and torque. Thanks to these conditions and the control scheme proposed in the following sections, it is possible to move the object like a non-holonomic vehicle.

We remark that an object with a complex shape can form a non-symmetric, non-holonomic vehicle geometry (see Fig. 3), and unlike a real non-holonomic vehicle, the object can move only forward. Given the desired non-holonomic velocity vector $(v, \omega)$ of a non-symmetric object, we can compute the pushing velocities as follows:

$$\mathbf{P}_L = \mathbf{G} + \mathbf{r}_L, \quad \mathbf{v}_L = \dot{\mathbf{G}} + \mathbf{w} \times \mathbf{r}_L \quad (12)$$
$$\mathbf{P}_R = \mathbf{G} + \mathbf{r}_R, \quad \mathbf{v}_R = \dot{\mathbf{G}} + \mathbf{w} \times \mathbf{r}_R \quad (13)$$

where $\mathbf{r}_L = [r_{Lx}, r_{Ly}, 0]^T$ and $\mathbf{r}_R = [r_{Rx}, r_{Ry}, 0]^T$ are the vectors from the mass center to the pushing points $\mathbf{P}_L$ and $\mathbf{P}_R$; where $\mathbf{v}_L$ and $\mathbf{v}_R$ are the velocities of the pushing points; where $\dot{\mathbf{G}} = v\,\mathbf{y}$ is the velocity of the mass center
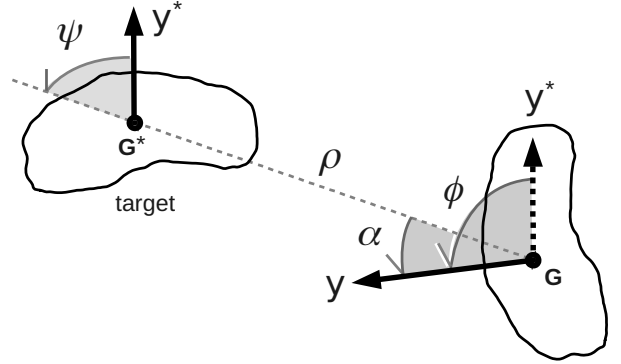


Fig. 4. State variables of the object with respect to a target pose.

with the unit vector $\mathbf{y} = [0, 1, 0]^T$ of the fixed motion direction and the linear speed $v$; and where $\mathbf{w} = \omega\,\mathbf{z}$ is the rotational velocity vector with the rotational axis $\mathbf{z} = [0, 0, 1]^T$ and the angular speed $\omega$. We can simplify and rewrite the pushing velocities for 2D planar space from (12) and (13) as below:

$$\mathbf{v}_L = \begin{bmatrix} 0 & -r_{Ly} \\ 1 & r_{Lx} \end{bmatrix} \begin{bmatrix} v \\ \omega \end{bmatrix}, \mathbf{v}_R = \begin{bmatrix} 0 & -r_{Ry} \\ 1 & r_{Rx} \end{bmatrix} \begin{bmatrix} v \\ \omega \end{bmatrix} \quad (14)$$

## IV. FORWARD NON-HOLONOMIC MOTION

In this section, we develop the kinematic model, the control law, and the constraints of an object with forward non-holonomic motion.

### A. Kinematics

Let the state vector of the object in polar coordinates be $\mathbf{x} = [\rho, \alpha, \phi]^T$ in the real world plane $\pi_W$ (See Fig. 4). Here, $\rho$ is the distance of the object to the desired position, $\phi$ is the alignment error of the object with respect to desired orientation, and $\alpha$ is the alignment error of the fixed motion direction of the object toward the desired position. Afterwards, let the desired motion of the object be the linear speed $v$ and the angular speed $\omega$, then the non-holonomic kinematics of the object can be written as follows:

$$\begin{bmatrix} \dot{\rho} \\ \dot{\alpha} \\ \dot{\phi} \end{bmatrix} = \begin{bmatrix} -\cos\alpha & 0 \\ \frac{1}{\rho}\sin\alpha & 1 \\ 0 & 1 \end{bmatrix} \begin{bmatrix} v \\ \omega \end{bmatrix} \quad (15)$$

## B. State Variables in the Similarity Space

Note that after transforming the measured image points by (9) and (11) from image plane $\pi_I$ to the similarity plane $\pi_{S(t_0)}$, we have the following relations between the state variables of the object expressed in planes $\pi_{S(t_0)}$ and $\pi_W$:

$$\bar{\rho} = k\,\rho\,, \qquad \bar{\alpha} = \alpha\,, \qquad \bar{\phi} = \phi \qquad (16)$$

where $\{\bar{\rho}, \bar{\alpha}, \bar{\phi}\} \in \pi_{S(t_0)}$, and $k$ is an unknown constant positive scale with known bounds $0 < k_{min} \leq k \leq k_{max}$. See Appendix D for the computation of bounds.

## C. Control Law

In this section we describe the proposed control law which is inspired from [16]. As said before, we need to adapt that control law from calibrated to uncalibrated framework, where the camera is now in eye-to-hand configuration instead of eye-in-hand, and it is applied to a system consisting of two mobile robots and an object instead of a single robot. We write this new control law (i.e., the desired motion) for this new system (i.e., object manipulation by pushing) from the computed state variables as follows:

$$v = k_\rho\,\bar{\rho}\,\cos\bar{\alpha}\,, \qquad (17)$$
$$\omega = k_\phi\,\bar{\phi} - k_\alpha\,\bar{\alpha} \qquad (18)$$

where $k_\rho$, $k_\alpha$, and $k_\phi$ are positive constant control gains. If the chosen control gains satisfy the following condition:

$$k_\alpha - k_\phi - k_{max}\,k_\rho > 0 \qquad (19)$$

where $k_{max}$ is the known upper bound of the unknown $k$, then the control law is locally exponentially stable. Again the control law, with gains satisfying (19), is globally asymptotically stable if the following condition also holds:

$$k_\alpha - 2\,k_\phi > 0\,. \qquad (20)$$

Proofs can be found in the Appendices A and B. Note that, contrary to [16], the stability analysis is performed here in the uncalibrated image space instead of the Euclidean space, which is known to be a difficult issue to solve in general.

We next obtain the input velocities of the pushing robots $\mathbf{v}_L$ and $\mathbf{v}_R$ from the desired motion of the object – the speeds $v$ and $\omega$ in (17) and (18) – using (14).

We would like to remark that these speeds are for non-holonomic vehicles so they can move forward and backward. In case of a pushed object, we should avoid backward motion since we cannot pull. Next subsection emphasizes the required conditions for forward motion maneuvers only.

## D. Forward Motion Conditions

In this section, we study the forward motion conditions of the system which should be satisfied during manipulation. The first condition that should hold for the state variables to guarantee the forward motion ($v \geq 0$) is as below:

$$|\bar{\alpha}| \leq \pi/2 \qquad \text{and} \qquad |\bar{\psi}| \leq \pi/2 \qquad (21)$$

where $\bar{\psi} = \bar{\phi} - \bar{\alpha}$. Condition (21) avoids cusps in the trajectory of the object which causes backward motion. This condition is guaranteed if we choose the motion direction $\mathbf{y}$ of the object in such a way that the maneuvers performed toward the target are minimized. In particular, this is done by minimizing the Lyapunov function $V(\bar{\mathbf{x}})$ – used in the stability proof of the control law in the Appendix B – at the initial configuration for $\bar{\alpha}$ subject to (21):

$$\min_{\bar{\alpha}} V(\bar{\mathbf{x}}) \text{ subject to } \bar{\alpha}^2 \leq \pi^2/4 \text{ and } \bar{\psi}^2 \leq \pi^2/4 \qquad (22)$$

In $\bar{\mathbf{x}}$, state variables $\bar{\rho}$ and $\bar{\phi}$ are known, and $\bar{\alpha}$ is unknown.

The second condition, that we should also impose while pushing the object, is to limit the angular speed of the object:

$$|\omega| \leq v\,/\,r \qquad (23)$$

where $r$ is the distance between a pushing point and the mass center of the object. This distance $r$ is computed as follows:

$$\text{if } \omega > 0 \text{ then } r = \|\mathbf{r}_L\| \text{ else } r = \|\mathbf{r}_R\| \qquad (24)$$

See Fig. 3. Condition (23) avoids pushing velocities $\mathbf{v}_L$ and $\mathbf{v}_R$ to have negative values along the motion axis $\mathbf{y}$, and it guarantees that we do not lose contact with the object. Condition (23) is satisfied if the following expressions hold:

$$\pi\,|\,2\,k_\phi - k_\alpha\,|\,/\,2 \leq \varepsilon_\alpha\,(k_{min}\,k_\rho\,\bar{\rho}_0\,/\bar{r} - k_\alpha) \qquad (25)$$

$$2\,(k_{max}\,k_\rho + k_\phi) \geq k_\alpha \qquad (26)$$

where $\bar{\rho}_0$ is the initial distance equal to $\bar{\rho}(t) \in \pi_{S(t_0)}$ when time was $t = 0$; where $\bar{r} = k\,r$ is the distance between the mass center and the corresponding pushing point of the object on the plane $\pi_{S(t_0)}$ with $k$ being equal to the one in (16); where $\varepsilon_\alpha$ is an arbitrary small positive angle; and where $k_{min}$ and $k_{max}$ are the known bounds of the unknown $k$. Proofs of (25) and (26) can be found in the Appendix C.

## V. RESULTS

We validated the pushing tasks with realistic simulation using V-REP free and open source software [19]. In simulations, an uncalibrated camera observes the scene from a fixed pose. Non-holonomic mobile robots are used for pushing. Figure 5 shows the simulation environment and the two non-holonomic mobile robots used for pushing the object.

We remark that a non-holonomic robot cannot push the object in every direction. It can push only along its fixed motion direction. Therefore, to be able to use non-holonomic robots to manipulate the object, we first choose two pushing points on the object such that points are at equal distance to the line defined by gravity center and the $y$-axis. This cancels the velocity components along the $\mathbf{x}$ axis of the object (see Fig. 3), and allows us to write the linear speeds of the mobile robots from (14):

$$v_L = v + r_{Lx}\,\omega \qquad v_R = v + r_{Rx}\,\omega \qquad (27)$$

Secondly, we correct the orientation of the non-holonomic mobile robots toward the pushing points (see Fig. 3) with a simple proportional control law given below:

$$\begin{bmatrix} \omega_L \\ \omega_R \end{bmatrix} = -k_\omega \begin{bmatrix} \alpha_L \\ \alpha_R \end{bmatrix}\,, \qquad k_\omega > 0 \qquad (28)$$
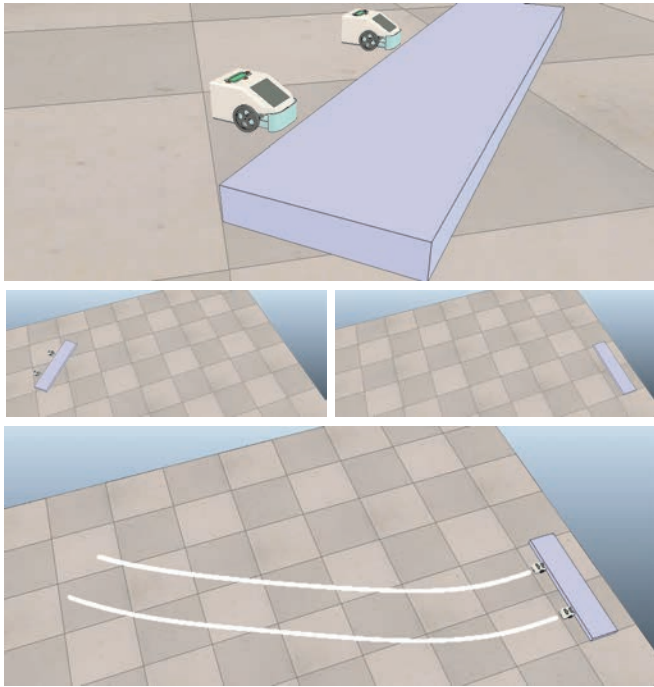
Fig. 5. V-REP simulation environment. Top image shows the two non-holonomic mobile robots and the box shaped object. Images in the middle row show an initial pose (left) and the target pose (right) from the uncalibrated camera viewpoint. At the bottom image, we see an example of the performed pushing task and the trajectories of the mobile robots.

where $\omega_L$ and $\omega_R$ are the computed angular speeds; $k_\omega$ is the positive control gain; and the $\alpha_L$ and $\alpha_R$ are the orientation errors of the non-holonomic mobile robots. Equation (28) keeps the non-holonomic mobile robots at the pushing points and orients them towards the correct motion direction of the object during the manipulation.

In simulations, we pushed a box shaped object from three different poses to the same target pose. The target pose is at $[x\,(m),\,y\,(m),\,\phi\,(deg)] = [0,\,0,\,0°]$ and the initial poses are at $[4,\,-6,\,-50°]$, $[2,\,-11,\,0°]$ and $[-3,\,-8,\,40°]$. Figure 6 shows these three pushing tasks. In this figure, each type of line represents a different simulation. For each one, the trace of the center of mass of the pushed box is represented with a thick line. The paths followed by the pushing robots are depicted with thin lines. The box in the initial and target poses is also depicted. It can be seen that the system evolves correctly to the desired state. An example of the results is provided in Fig. 5, where the traces of the two pushing robots are plotted in white. Figure 7 shows the evolution of the linear $v$ and angular $\omega$ speeds of the object versus time during these three pushing tasks. Figure 8 shows the evolution of the state variables $\bar{\rho}$ and $\bar{\phi}$ of the object versus time during these three pushing tasks. Note that the control fails if the proposed constraints are violated when defining the control setup or reaching the target location requires several manoeuvres. In that case, the system cannot reach the target location because of robots losing contact with the object. Supplementary illustration of the simulations is provided by the video that accompany the paper.
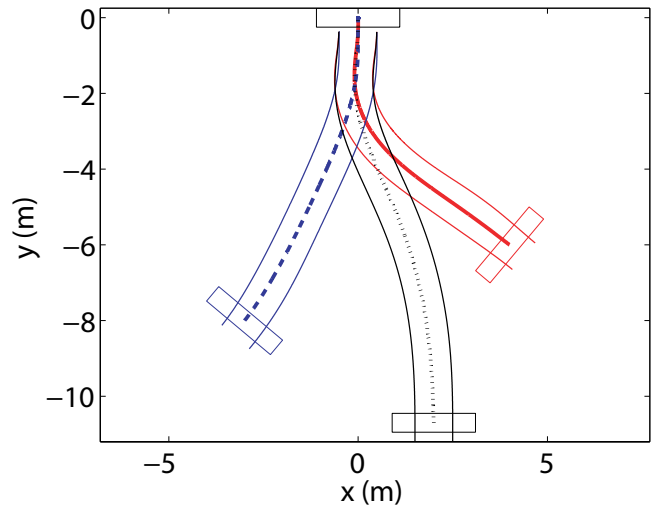


Fig. 6. Three different initial poses of the object and its maneuvers toward the target pose at the origin $(0, 0)$ in the V-REP simulation environment.
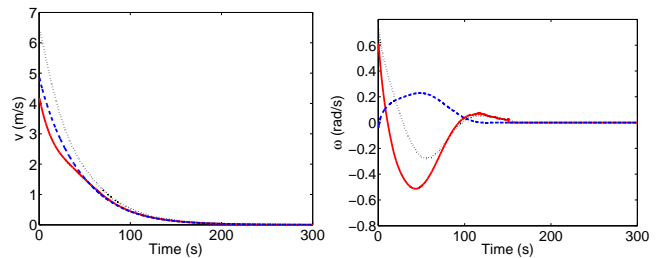


Fig. 7. Evolution of the linear $v$ and angular $\omega$ speeds of the object versus time. Each different line corresponds to one of the simulations in Fig. 6.

## VI. CONCLUSIONS

This paper proposed, for the first time, an uncalibrated visual servoing scheme to pose objects in the plane by pushing with two non-holonomic mobile robots under non-holonomic velocity constraint. Our method yields smooth and efficient trajectories with guaranteed stability. This scheme is then validated by realistic simulation results obtained with V-REP software. Regarding possible directions for future work, one idea that can be addressed is how to automatically select the points to push in the border of a convex object with arbitrary shape. It would be also interesting to study the possibility of extending the presented method to robot manipulators for the pushing task instead of using mobile robots.
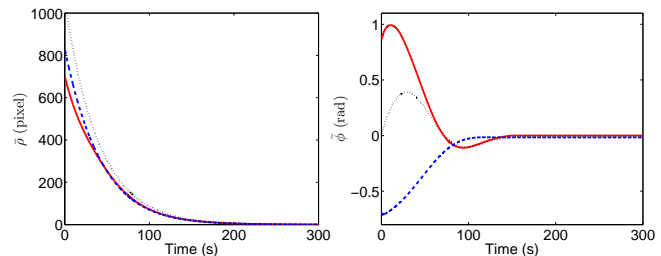


Fig. 8. Evolution of the state variables $\bar{\rho}$ and $\bar{\phi}$ of the object versus time for the simulations shown in Fig. 6.

## A. Local Exponential Stability of the Control Law

Using (16), (17) and (18) in (15), we can obtain the closed-loop system described as below:

$$
\begin{aligned}
\dot{\bar{\rho}} &= -k_\rho \, k \, \bar{\rho} \, \cos^2 \bar{\alpha} \\
\dot{\bar{\alpha}} &= k_\phi \, \bar{\phi} - k_\alpha \, \bar{\alpha} + k_\rho \, k \, \cos \bar{\alpha} \sin \bar{\alpha} \\
\dot{\bar{\phi}} &= k_\phi \, \bar{\phi} - k_\alpha \, \bar{\alpha}
\end{aligned}
\tag{29}
$$

The first-order Taylor series approximation of this closed-loop system (29) around the equilibrium state gives the following linearized system:

$$
\begin{bmatrix} \dot{\bar{\rho}} \\ \dot{\bar{\alpha}} \\ \dot{\bar{\phi}} \end{bmatrix} \approx
\begin{bmatrix}
-k \, k_\rho & 0 & 0 \\
0 & k \, k_\rho - k_\alpha & k_\phi \\
0 & -k_\alpha & k_\phi
\end{bmatrix}
\begin{bmatrix} \bar{\rho} \\ \bar{\alpha} \\ \bar{\phi} \end{bmatrix}
\tag{30}
$$

This system is locally exponentially stable if and only if the eigenvalues of the linearized system matrix are negative. This yields the condition (19). Therefore, satisfying (19) is sufficient for local exponential stability.

## B. Global Stability of the Control Law

The closed-loop system (29) with control gains selected following (19) is globally asymptotically stable if (20) holds.

*Proof:* We define the Lyapunov function as

$$
V(\bar{\mathbf{x}}) = \bar{\mathbf{x}}^T \, \mathbf{P} \, \bar{\mathbf{x}} + \frac{1}{2} \, \sin^2 \bar{\alpha} \,,
\tag{31}
$$

where $V(\bar{\mathbf{x}}) > 0$ for all $\bar{\mathbf{x}} \neq 0$, with

$$
\mathbf{P} = \frac{1}{2 \, k_\rho}
\begin{bmatrix}
1 & 0 & 0 \\
0 & k_\phi & -k_\phi \\
0 & -k_\phi & k_\phi
\end{bmatrix} \,.
\tag{32}
$$

The derivative of (31) yields

$$
\begin{aligned}
\dot{V} &= \bar{\alpha} \, \sin \bar{\alpha} \cos \bar{\alpha} \, \Big( k_\phi + k_\rho \frac{\sin \bar{\alpha} \cos \bar{\alpha}}{\bar{\alpha}} - k_\alpha \Big) \\
&\quad - \bar{\rho}^2 \, \cos^2 \bar{\alpha} \,.
\end{aligned}
\tag{33}
$$

It can be seen that $\dot{V} < 0$ for all $\bar{\alpha} \in (-\pi/2, \, \pi/2)$ if the following constraint holds:

$$
k_\alpha - k_\phi - (k_\rho \, \sin \bar{\alpha} \cos \bar{\alpha})/\bar{\alpha} > 0 \,.
\tag{34}
$$

Since $(\sin \bar{\alpha} \cos \bar{\alpha})/\bar{\alpha}$ is bounded by 1, constraint (34) leads to (19). We next study the case of $\bar{\alpha} = \pm \pi/2$, which results in $\dot{V} = 0$. In this case, we check the derivative of $\bar{\alpha}$ in (29).

$$
\dot{\bar{\alpha}}(\bar{\alpha} = \pm \pi/2) = \mp k_\alpha \, \pi/2 + k_\phi \, \bar{\phi} \,.
\tag{35}
$$

We can ensure that $\dot{\bar{\alpha}} < 0$ when $\bar{\alpha} = \pi/2$, and $\dot{\bar{\alpha}} > 0$ when $\bar{\alpha} = -\pi/2$, if the following constraint holds:

$$
-k_\alpha + \frac{2}{\pi} \, k_\phi \, \bar{\phi} < 0 \,, \quad k_\alpha + \frac{2}{\pi} \, k_\phi \, \bar{\phi} > 0 \,.
\tag{36}
$$

If the maximum bounds of $\bar{\phi}$ are considered, i.e. $\bar{\phi} = \pm \pi$ respectively, we obtain constraint (20). Therefore, the regulated system is asymptotically stable for all $\bar{\alpha} \in [-\pi/2, \, \pi/2]$.

In order to show the region of attraction of the equilibrium $\bar{\mathbf{x}} = \mathbf{0}$ is global, we also analyze the case of

$\bar{\alpha} \in [-\pi, -\pi/2] \cup [\pi/2, \pi]$. By checking the derivative of $\bar{\alpha}$ in (29) we have

$$
\bar{\alpha} \in [\pi/2, \pi] \Rightarrow \quad \dot{\bar{\alpha}} < 0 \Leftrightarrow -\tfrac{\pi}{2} \, k_\alpha + k_\phi \, \bar{\phi} < 0 \,, \tag{37}
$$
$$
\bar{\alpha} \in [-\pi, -\pi/2] \Rightarrow \quad \dot{\bar{\alpha}} > 0 \Leftrightarrow \tfrac{\pi}{2} \, k_\alpha + k_\phi \, \bar{\phi} > 0 \,. \tag{38}
$$

where the most unfavorable case of $\bar{\alpha}$ is used. These previous constraints yields to constraint (20) when the maximum bounds of $\bar{\phi}$ are included. Thus, the global asymptotic stability of the regulated system (29) is guaranteed if constraints (19) and (20) holds. ∎

## C. Viability of the Angular Speed Condition

We can rewrite the angular speed condition $|\omega| \leq v/r$ using (16), (17) and (18) as follows:

$$
\big| k_\phi \, \bar{\phi} - k_\alpha \, \bar{\alpha} \big| \leq k \, k_\rho \, \bar{\rho} \cos \bar{\alpha} \, / \, \bar{r}
\tag{39}
$$

The worst case, which violates the above condition, happens for $\bar{\alpha} = \pm \pi/2$ when the motion direction of the object is orthogonal to the direction towards the target. In this case, $v = 0$ and the condition $|\omega| \leq v/r$ is violated. This is a singular case that can be avoided in practice by, for example, applying the proposed solution for motion direction selection (22). We thus set the worst case as $\bar{\alpha} = \pm \pi/2 \mp \varepsilon_\alpha$ where $\varepsilon_\alpha$ is an arbitrary small positive angle. Addition of $\pm \varepsilon_\alpha$ to $\bar{\alpha}$ also keeps $v > 0$.

Regarding $\bar{\phi}$, it can be deduced that the worst case corresponds to $\bar{\phi} = \pm \pi$. This happens when the motion direction of the object is oriented backward with respect to desired configuration. Equation (39) can then be rewritten for the worst case values of $\bar{\alpha}$, $\bar{\phi}$ and $k$ as (25). We also assumed that $\sin(\pm \varepsilon_\alpha) \approx \pm \varepsilon_\alpha$.

Condition (25) allows tuning the control gains to avoid control law saturation during the beginning of the motion period. Nevertheless, it does not guarantee $|\omega| \leq v/r$ at the end of the motion period, when $v$ tends to zero. In that case, we must guarantee that the convergence rate of $\omega$ is higher than $v$. This case appears when the system is getting closer to the equilibrium state, therefore here for analysis, we can consider the first-order Taylor series approximation of the closed-loop system given in (30). The eigenvalues of this system are as follows:

$$
\lambda_\rho = -k \, k_\rho \,, \quad \lambda_{\alpha,\phi} = \frac{-k_L \mp \sqrt{(k_L)^2 - 4 \, k \, k_\rho k_\phi}}{2}
\tag{40}
$$

where $k_L = k_\alpha - k_\phi - k \, k_\rho$. Since the convergence rates of the state variables are given by their eigenvalues, e.g.:

$$
\bar{\rho}(t) = \bar{\rho}_0 \, e^{(\lambda_\rho t)} \quad \text{thus} \quad v \approx k_\rho \, \bar{\rho}_0 \, e^{(\lambda_\rho t)}
\tag{41}
$$

we derive the conditions for (40) such that $|\lambda_\rho|$ is the smallest eigenvalue. In particular, we look for the following condition:

$$
|\lambda_\alpha| \geq |\lambda_\phi| > |\lambda_\rho|
\tag{42}
$$

We can deduce from (40) and (42) the following expression:

$$
2 \, (k_{max} \, k_\rho + k_\phi) \geq k_\alpha
\tag{43}
$$

where $k_{max}$ is again the upper bound of the unknown constant positive scale $k$. We can thus sustain the angular speed condition given in (23) by satisfying (25) and (43).

### D. Boundedness of Lengths in the Image Plane

Perspective projection scales/foreshortens a length of an object to a smaller length. Physical world lengths can then be related to the image plane lengths from the ratios of similar triangles:

$$\bar{\rho} \approx \frac{f}{Z}\,\rho \qquad \text{with} \qquad \frac{f}{Z} < 1 \qquad (44)$$

where $f$ is the unknown focal length of the uncalibrated camera, and $Z$ is the unknown distance of the line segment – located between the current and target positions of the pushed object in the support plane– to the optical center of the uncalibrated camera. As long as the objects are visible to the camera, the $Z$ is greater than the $f$. In equation (44), $\rho$ and $\bar{\rho}$ are expressed in the same metric units. The metric unit can be chosen arbitrarily (e.g., m, $\mu m$). Expressing metric units in microns $-\mu m-$ and knowing that the state-of-the-art smallest CCD/CMOS sensor pixel size $s$ is about a few microns ($s > 1\,\mu m$), we can rewrite (44) for $\bar{\rho}$ expressed in pixels as follows:

$$\bar{\rho} \approx \frac{1}{s}\,\frac{f}{Z}\,\rho \qquad \text{with} \qquad \frac{1}{s} < 1 \qquad (45)$$

This time in (45), $\rho$ is in microns and $\bar{\rho}$ is in pixels. We rewrite (45) as below:

$$\bar{\rho} \approx T_\rho\,\rho \qquad \text{with} \qquad T_\rho = \frac{1}{s}\,\frac{f}{Z} < 1 \qquad (46)$$

where $T_\rho$ is the unknown scale. This unknown scale then can be bounded as follows:

$$0 < T_{min} \leq T_\rho \leq T_{max} < 1 \qquad (47)$$

Finally, one can choose $T_{min}$ and $T_{max}$ regarding (47) and compute $k_{min}$ and $k_{max}$ as below:

$$k_{min} = S_E\,T_{min}\,, \qquad k_{max} = S_E\,T_{max} \qquad (48)$$

where $S_E$ is a known scale extracted from $\mathbf{E}_S$ (10).

### REFERENCES

[1] M. T. Mason, "Mechanics and planning of manipulator pushing operations," *The International Journal of Robotics Research*, vol. 5, no. 3, pp. 53–71, 1986.

[2] M. A. Peshkin and A. C. Sanderson, "Planning robotic manipulation strategies for workpieces that slide," *IEEE Journal of Robotics and Automation*, vol. 4, no. 5, pp. 524–531, Oct. 1988.

[3] Z. Balorda and T. Bajd, "Reducing positioning uncertainty of objects by robot pushing," *IEEE Transactions on Robotics and Automation*, vol. 10, no. 4, pp. 535–541, Aug. 1994.

[4] S. Akella and M. T. Mason, "Posing polygonal objects in the plane by pushing," *The International Journal of Robotics Research*, vol. 17, no. 1, pp. 70–88, 1998.

[5] Q. Li and S. Payandeh, "Manipulation of convex objects via two-agent point-contact push," *The International Journal of Robotics Research*, vol. 26, no. 4, pp. 377–403, 2007.

[6] M. A. Peshkin and A. C. Sanderson, "The motion of a pushed, sliding workpiece," *IEEE Journal of Robotics and Automation*, vol. 4, no. 6, pp. 569–598, Dec. 1988.

[7] K. M. Lynch, "The mechanics of fine manipulation by pushing," in *IEEE International Conference on Robotics and Automation*, vol. 3, May 1992, pp. 2269–2276.

[8] F. Gandolfo, M. Tistarelli, and G. Sandini, "Visual monitoring of robot actions," in *Workshop on Intelligence for Mechanical Systems. IEEE/RSJ International Conference on Intelligent Robots and Systems*, vol. 1, Nov. 1991, pp. 269–275.

[9] Y. Okawa and K. Yokoyama, "Control of a mobile robot for the push-a-box operation," in *IEEE International Conference on Robotics and Automation*, May 1992, pp. 761–766 vol.1.

[10] M. Salganicoff, G. Metta, A. Oddera, and G. Sandini, "A direct approach to vision guided manipulation," in *International Conference on Advanced Robotics*, Nov. 1993.

[11] M. A. Golkar, S. T. Namin, and H. Aminaiee, "Fuzzy controller for cooperative object pushing with variable line contact," in *IEEE International Conference on Mechatronics*, Apr. 2009, pp. 1–6.

[12] S. Akella and M. T. Mason, "Using partial sensor information to orient parts," *International Journal of Robotics Research*, vol. 18, no. 10, pp. 963–997, Oct. 1999.

[13] A. Sudsang, F. Rothganger, and J. Ponce, "Motion planning for disc-shaped robots pushing a polygonal object in the plane," *IEEE Transactions on Robotics and Automation*, vol. 18, no. 4, pp. 550–562, Aug. 2002.

[14] G. A. S. Pereira, M. F. M. Campos, and V. Kumar, "Decentralized algorithms for multi-robot manipulation via caging," *The International Journal of Robotics Research*, vol. 23, no. 7-8, pp. 783–795, 2004.

[15] D. Rus, B. Donald, and J. Jennings, "Moving furniture with teams of autonomous robots," in *IEEE/RSJ International Conference on Intelligent Robots and Systems*, vol. 1, Aug. 1995, pp. 235–242.

[16] G. López-Nicolás and C. Sagüés, "Vision-based exponential stabilization of mobile robots," *Autonomous Robots*, vol. 30, pp. 293–306, 2011.

[17] O. Faugeras, "Stratification of three-dimensional vision: projective, affine, and metric representations," *Journal of the Optical Society of America A*, vol. 12, no. 3, pp. 465–484, 1995.

[18] Q. Li and S. Payandeh, "Modeling and analysis of dynamic multi-agent planar manipulation," in *IEEE International Symposium on Computational Intelligence in Robotics and Automation*, 2001, pp. 200–205.

[19] E. Rohmer, S. P. N. Singh, and M. Freese, "V-rep: A versatile and scalable robot simulation framework," in *IEEE/RSJ International Conference on Intelligent Robots and Systems*, Nov. 2013, pp. 1321–1326.